THE JOURNAL OF BIOLOGICAL CHEMISTRY
Vol. 279, No. 36, Issue of September 3, pp. 37734–37740, 2004

Printed in U.S.A.

Structure-Activity Relationships of Hainantoxin-IV and Structure Determination of Active and Inactive Sodium Channel Blockers*

Received for publication, May 24, 2004, and in revised form, June 15, 2004
Published, JBC Papers in Press, June 16, 2004, DOI 10.1074/jbc.M405765200

Dongling Li‡, Yucheng Xiao§, Xia Xu§, Xia Xiong§, Shanyun Lu‡, Zhonghua Liu§, Qi Zhu§, Meichi Wang§, Xiaocheng Gu‡, and Songping Liang§¶

From the ‡College of Life Sciences, Peking University, Beijing 100871 and the §College of Life Sciences, Hunan Normal University, Changsha 410081, People's Republic of China

Hainantoxin-IV (HNTX-IV) can specifically inhibit the neuronal tetrodotoxin-sensitive sodium channels and defines a new class of depressant spider toxin. The sequence of native HNTX-IV is ECLGFGKGCNPSNDQC-CKSSNLVCSRKHRWCKYEI-NH_2. In the present study, to obtain further insight into the primary and tertiary structural requirements of neuronal sodium channel blockers, we determined the solution structure of HNTX-IV as a typical inhibitor cystine knot motif and synthesized four mutants designed based on the predicted sites followed by structural elucidation of two inactive mutants. Pharmacological studies indicated that the S12A and R26A mutants had activities near that of native HNTX-IV, while K27A and R29A demonstrated activities reduced by 2 orders of magnitude. ^{1}H MR analysis showed the similar molecular conformations for native HNTX-IV and four synthetic mutants. Furthermore, in the determined structures of K27A and R29A, the side chains of residues 27 and 29 were located in the identical spatial position to those of native HNTX-IV. These results suggested that residues Ser^{12}, Arg^{26}, Lys^{27}, and Arg^{29} were not responsible for stabilizing the distinct conformation of HNTX-IV, but Lys^{27} and Arg^{29} were critical for the bioactivities. The potency reductions produced by Ala substitutions were primarily due to the direct interaction of the essential residues Lys^{27} and Arg^{29} with sodium channels rather than to a conformational change. After comparison of these structures and activities with correlated toxins, we hypothesized that residues Lys^{27}, Arg^{29}, His^{28}, Lys^{32}, Phe^{5}, and Trp^{30} clustered on one face of HNTX-IV were responsible for ligand binding.

Voltage-gated sodium channels (VGSCs)[1] play an essential role in the initiation and propagation of the action potentials in excitable cells. They are composed of a functional pore-forming α subunit (260 kDa) associated with up to four auxiliary β subunits (1–4). To date, at least six different receptor sites have been identified on VGSCs by different neurotoxins, but most spider toxins targeting insect and mammalian neuronal sodium channels have a common mode of action similar to that of scorpion α-toxins. They slow or block sodium channel inactivation (5, 6).

A relatively new family of spider toxins has been discovered that inhibit tetrodotoxin-sensitive (TTX-S) sodium currents, blocking most likely at site 1 of neuronal VGSCs (7–9). Hainantoxin-IV (HNTX-IV) is a 35-amino acid residue blocker of sodium channels that was isolated from the venom of the Chinese bird spider *Ornithoctonus hainana* Liang (=*Selenocosmia hainana* Liang) (7). It has been shown to specifically inhibit the neuronal TTX-S VGSCs with an IC_{50} value of 34.0 nM in adult rat dorsal root ganglion (DRG) neurons and seem to interact with neurotoxin receptor site 1 through a mechanism quite similar to that of TTX (10) without affecting the activation and inactivation kinetics. The toxin has a high proportion of basic residues, and it is cross-linked by three conserved intramolecular disulfide bonds. The linkage pattern of disulfide bridges in HNTX-IV is I-IV, II-V, and III-VI (Cys^2-Cys^{17}, Cys^9-Cys^{24}, and Cys^{16}-Cys^{31}) as assigned by partial reduction and sequence analysis. The synthetic HNTX-IV demonstrated the same disulfide pairings and biological activity as the native HNTX-IV, so the possibility that a very potent minor contaminant was present was ruled out (11).

Among 28 spider peptides or homologues acting on VGSCs from the PubMed data base (www.pubmed.com), another four toxins from the venom of the Chinese bird spiders were found to not affect the activation and inactivation kinetics of Na^+ channel. HNTX-I blocks $rNa_v1.2/\beta_1$ and the insect Na^+ channel para/tipE (12), while the other three toxins (HNTX-III and -V and HWTX-IV) inhibit TTX-S Na^+ currents in adult rat DRG neurons similar to HNTX-IV (7–9). HNTX-IV is closely related in primary sequence to HNTX-III and -V and HWTX-IV, and they all have the same numbers and linkage modes of disulfide bonds (Fig. 1). However, these toxins show no significant sequence homology to any other known neurotoxins. So the four spider toxins (HNTX-III–V and HWTX-IV) define a new class of spider toxins affecting VGSCs. The three-dimensional solution structure of HWTX-IV has been determined using two-dimensional ^{1}H NMR spectroscopy, and it was hypothesized that the positively charged residues of loop IV (residues 25–29), espe-

* This work was supported by National Natural Science Foundation of China under Contract No. 30170193 39990 600. The costs of publication of this article were defrayed in part by the payment of page charges. This article must therefore be hereby marked "*advertisement*" in accordance with 18 U.S.C. Section 1734 solely to indicate this fact.

The atomic coordinates and structure factors (code 1NIY (native HNTX-IV), 1RYV (K27A), and 1RYG (R29A)) have been deposited in the Protein Data Bank, Research Collaboratory for Structural Bioinformatics, Rutgers University, New Brunswick, NJ (http://www.rcsb.org/).

The ^{1}H chemical shifts have been deposited in BioMagResBank (BMRB) with accession codes 5676, 6066, and 6067, respectively.

¶ To whom correspondence should be addressed. Tel.: 86-731-8861304; Fax: 86-731-8861304; E-mail: liangsp@hunnu.edu.cn.

[1] The abbreviations used are: VGSC, voltage-gated sodium channel; HNTX, hainantoxin; TTX, tetrodotoxin; TTX-S, TTX-sensitive; DRG, dorsal root ganglion; NOE, nuclear Overhauser effect; HPLC, high pressure liquid chromatography; DQF-COSY, double quantum-filtered correlation spectroscopy; TOCSY, total correlated spectroscopy; NOESY, nuclear Overhauser effect spectroscopy; MALDI-TOF, matrix-assisted laser desorption/ionization time-of-flight; HWTX, huwentoxin; Fmoc, *N*-(9-fluorenyl)methoxycarbonyl; TBTU, 2-(1*H*-benzotriazol-1-yl)-1,1,3,3-tetramethyluronium tetrafluoroborate; HOBt, hydroxybenzotriazole; NMM, *N*-methylmorpholine; r.m.s., root mean square.

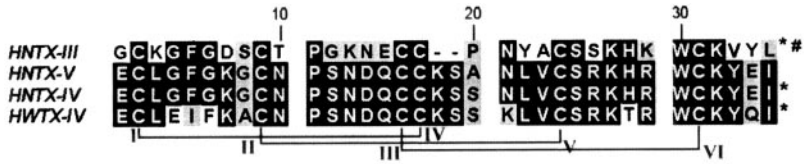

FIG. 1. **Comparison of the amino acid sequence of HNTX-IV with previously described neuronal TTX-S VGSC blockers from the venom of the Chinese bird spider *Selenocosmia*.** * represents an amidated carboxyl terminus. # shows the sequence of HNTX-III from the Swiss-Prot knowledge base under accession number P83464. Identical residues and conservatively substituted residues are shaded in *black* and *gray*, respectively. The disulfide bridge pattern of these toxins is indicated *below* the sequences.

cially Arg^{26}, were crucial to its binding to the neuronal TTX-S VGSCs (8). However, this hypothesis has not been supported by the results of experiments with mutants. On the other hand, there is also no structural information available on HNTX-IV. Determination of the structure of HNTX-IV is therefore important to gain further information regarding the design of synthetic analogues for the structure-activity relationships of these toxins.

In the present study, we determined the solution structure of HNTX-IV by ^{1}H NMR with distance geometry and simulated annealing. Based on the structural comparison and sequence assignment with other related toxins, we hypothesized that the positively charged residues Arg^{26}, Lys^{27}, and Arg^{29} in loop IV and vicinal polar residue Ser^{12} clustered on one face of HNTX-IV may be the potential interaction site. Mutants S12A, R26A, K27A, and R29A were synthesized by solid-phase Fmoc chemistry followed by oxidative refolding of purified peptides under the optimal conditions. ^{1}H NMR analysis showed similar molecular conformations for native HNTX-IV and synthetic mutants. Pharmacological studies indicated that residues Ser^{12} and Arg^{26} were not important for the activities, while Lys^{27} and Arg^{29} were critical for the bioactivities. These results provide useful information for structure-activity relationships of toxins like HNTX-IV.

EXPERIMENTAL PROCEDURES

NMR Spectroscopy of Native HNTX-IV—An NMR sample was prepared by dissolving the native HNTX-IV in 500 μl of 20 mM deuterium sodium acetate buffer (H_2O/D_2O, 9:1, v/v) containing 0.002% NaN_3 and 0.01 mM EDTA with a final concentration of 5.5 mM HNTX-IV and a pH of 4.0. Sodium 3-(trimethylsilyl)propionate-2,2,3,3-d_4 was added to a final concentration of 200 μM as an internal chemical shift reference. For experiments in D_2O, the sample used in H_2O experiments was lyophilized and then redissolved in 500 μl of 99.996% D_2O (Cambridge Isotope Laboratories).

All NMR spectra were observed on a 500-MHz Bruker DRX-500 spectrometer with a sample temperature of 295 K. Several sets of two-dimensional spectra were recorded in a phase-sensitive mode by the time-proportional phase incrementation method following standard pulse sequences and phase cycling. TOCSY spectra were obtained with a mixing time of 85 ms. NOESY spectra were recorded in D_2O with a mixing time of 200 ms and in H_2O with mixing times of 100, 200, and 400 ms. Solvent suppression was achieved by the presaturation method. All two-dimensional measurements were recorded with 1024 × 512 frequency data points and were zero-filled to yield 2048 × 1024 data matrices except for the high resolution DQF-COSY spectrum. The DQF-COSY spectrum was recorded with 2048 × 1024 data points in the t2 and t1 dimensions, respectively, and zero-filled to 4096 × 2048 points to measure the coupling constants. All spectra were processed and analyzed using Felix 98.0 (Biosym Technologies) software running on a Silicon Graphics O2 work station. Before Fourier transformation, the signal was multiplied by a sine bell or sine bell square window functions with a $\pi/2$ phase shift.

The hydrogen-deuterium exchange experiments were carried out by recording a series of one-dimensional spectra after the lyophilized sample was redissolved in D_2O. A TOCSY spectrum was recorded after 2 h of exchange.

Structure Calculations of Native HNTX-IV—Distance constraints were obtained from the intensities of cross-peaks in NOESY spectra with a mixing time of 200 ms. All NOE data were classified into four distance ranges: 1.8–2.7, 1.8–3.5, 1.8–5.0, and 1.8–6.0 Å, corresponding to strong, medium, weak, and very weak NOE values, respectively. Pseudoatom corrections were applied to non-stereospecifically assigned methyl and methylene protons according to the method of Wüthrich (13).

Fourteen ϕ dihedral angle restraints derived from $^3J_{NH\text{-}C\alpha H}$ coupling constants were restrained to $-120° \pm 30$ for $^3J_{NH\text{-}C\alpha H} \geq 8.80$ Hz and $-65° \pm 25$ for $^3J_{NH\text{-}C\alpha H} \leq 5.50$ Hz. HNTX-IV contains 6 cysteine residues paired as Cys^2-Cys^{17}, Cys^9-Cys^{24}, and Cys^{16}-Cys^{31} as assigned by partial reduction and sequence analysis. Three distance constraints for each disulfide bond were $S(i) - S(j)$, $S(i) - C_\beta(j)$, and $S(j) - C_\beta(i)$ whose target values were set to 2.02 ± 0.02, 2.99 ± 0.5, and 2.99 ± 0.5 Å, respectively. Eight hydrogen bond constraints confined the $NH(i) - O(j)$ and $N(i) - O(j)$ distance as 1.8–2.7 and 2.8–3.7 Å, respectively, according to slowly exchanging amide protons and NOE patterns. Structural calculations were performed with 583 distance constraints and 14 dihedral angle constraints using the standard protocol of the X-PLOR 3.851 program (14).

Peptide Synthesis, Folding, and Purification—Mutants S12A, R26A, K27A, and R29A were synthesized starting from a poly(ethylene glycol)polystyrene resin equipped with a peptide amide linker (Fmoc-peptide amide linker-polyethylene glycol-polystyrene (PAL-PEG-PS) amide resin, Applied Biosystems) on an automatic peptide synthesizer (PerSeptive Biosystems) using an Fmoc/*tert*-butyl strategy and HOBt/TBTU/NMM coupling method. All amino acids were purchased from Chemassist Corp., and side chains were protected as follows: trityl for Asn, Cys, His, and Gln; *tert*-butyl ester for Asp and Glu; *tert*-butyl ether for Ser and Tyr; 2,2,4,6,7-pentamethyldihydrobenzofuran-5-sulfonyl for Arg; and *tert*-butyloxycarbonyl for Lys. Peptide synthesis was accomplished on a 0.10-mmol scale. The terminal Fmoc group was removed by treatment with 1:4 piperidine/*N*,*N*-dimethylformamide (v/v). After completion of synthesis, the peptide was cleaved from the resin with simultaneous removal of side chain protective groups by treatment with reagent K (82.5% trifluoroacetic acid, 5% double distilled H_2O, 5% phenol, 5% thioanisole, and 2.5% ethanedithiol) for 2 h at room temperature. The resin was then filtered, and the free peptide was precipitated in cold ether at 4 °C. After centrifugation and washing once with cold ether, the peptide was dissolved in 20% acetic acid and lyophilized. The reduced peptides were purified by semipreparative reverse-phase HPLC using a 60-min linear gradient of 10–50% eluent B (0.1% trifluoroacetic acid in acetonitrile) in eluent A (0.1% trifluoroacetic acid in double distilled H_2O) over 60 min on a column (1.0 × 25 cm) at 3 ml/min flow rate. Peaks were analyzed by analytical HPLC, and more than 95% pure fractions were pooled and lyophilized.

The linear peptides were oxidized with glutathione and purified using the method recently described by Zhuqi (15). The molecular weights of the reduced peptides or oxidized peptides were checked by matrix-assisted laser desorption/ionization time-of-flight (MALDI-TOF) mass spectrometry on a Voyager-DE™ STR Biospectrometry™ work station. For each analogue, the measured molecular mass corresponded to the predicted value within 1.0 unit, consistent with the correctness of the sequence and the complete removal of all side chain protection groups.

Electrophysiological Experiments—The whole cell patch clamp experiments were made from rat DRG neurons as described previously (7). Rat DRG neurons were acutely dissociated and maintained in a short term primary culture using the method described by Hu and Li (16). Briefly 30-day-old adult Sprague-Dawley rats of either sex were killed by decapitation, and the dorsal root ganglia were isolated quickly from the spinal cord. Then they were transferred into Dulbecco's modified eagle's medium containing trypsin (0.5 mg/ml, type III, Sigma), collagenase (1.0 mg/ml, type IA, Sigma), and DNase (0.1 mg/ml, type III, Sigma) to incubate at 34 °C for 30 min. Trypsin inhibitor (1.5 mg/ml, type II-S, Sigma) was used to terminate enzyme treatment. The DRG cells were transferred into 35-mm dishes (Corning, Sigma) with the culture medium and incubated in a CO_2 incubator (5% CO_2, 95% air at

TABLE I
Structural statistics for 20 structures of native HNTX-IV, K27A, and R29A

Parameters	Native HNTX-IV	K27A	R29A
Experimental constraints			
Intraresidue NOE ($i - j = 0$)	190	171	156
Sequential NOE ($\|i - j\| = 1$)	139	90	94
Medium range NOE ($\|i - j\| \leq 5$)	61	33	35
Long range NOE ($\|i - j\| \geq 5$)	176	105	103
Dihedral angle (ϕ)	14	13	15
Average potential energies (kcal mol^{-1})[a]			
E_{total}	−67.64 ± 5.470	−55.24 ± 6.668	−47.78 ± 6.583
E_{bond}	5.518 ± 0.426	5.452 ± 0.400	5.574 ± 0.260
E_{angle}	42.24 ± 0.814	39.76 ± 0.860	42.12 ± 0.923
$E_{improper}$	4.787 ± 0.183	4.731 ± 0.162	4.698 ± 0.117
E_{vdW}	−120.53 ± 5.445	−105.81 ± 6.329	−101.02 ± 6.346
E_{NOE}	0.323 ± 0.161	0.613 ± 0.150	0.786 ± 0.264
E_{cdih}	0.017 ± 0.031	0.012 ± 0.015	0.039 ± 0.041
r.m.s. deviation from experimental constraints[b]			
NOE distance (Å)	0.003 ± 0.001	0.005 ± 0.001	0.006 ± 0.001
Dihedral angle (°)	0.097 ± 0.08	0.097 ± 0.081	0.175 ± 0.117
r.m.s. deviations from idealized geometry[a]			
Bonds (Å)	0.003 ± 0.0001	0.003 ± 0.0001	0.003 ± 0.0001
Angles (°)	0.533 ± 0.005	0.523 ± 0.005	0.538 ± 0.006
Impropers (°)	0.330 ± 0.006	0.331 ± 0.006	0.332 ± 0.004
Average r.m.s. differences versus mean structure (Å)			
Backbone atoms (N, Cα, and C)	0.485 ± 0.064	0.620 ± 0.097	0.643 ± 0.111
Non-hydrogen heavy atoms	1.229 ± 0.131	1.313 ± 0.130	1.327 ± 0.129
Pairwise r.m.s. differences of 20 structures (Å)			
Backbone atoms (N, Cα, and C)	0.689 ± 0.124	0.901 ± 0.159	0.925 ± 0.183
Non-hydrogen heavy atoms	1.746 ± 0.192	1.871 ± 0.215	1.874 ± 0.212

[a] The idealized geometry and energy values were defined by the CHARMM force field as implemented in the XPLOR program. All statistical values of energies, r.m.s. deviations, and r.m.s. differences are given as the mean ± S.D.

[b] The statistics of experimental r.m.s. deviation of NOE and dihedral angle constraints were from the calculation with force constants of 50 kcal mol^{-1} Å^{-2} and 200 kcal mol^{-1} radian^{-2}, respectively.

37 °C) for 1–4 h before the patch clamp experiment.

Patch clamp experiments were performed at room temperature (20–25 °C) under the whole cell patch clamp configuration. Patch pipettes (2–3-μm diameter) were pulled from borosilicate glass capillary tubing by using a two-step vertical puller (PC-10, Narishige, Olypmus) and heat-polished with a microforge (MF-900, Narishige). Patch pipettes with resistances of 1.0–2.0 megaohms were used. The series resistance was compensated 65–70%, and linear capacitative and linear leakage currents were digitally subtracted by a P/4 procedure. Sodium currents were filtered at 10 kHz and digitized at 3 kHz with an EPC-9 patch clamp amplifier (HEKA Electronics, Germany). Experimental data were collected and analyzed by using the program Pulse/Pulsefit 8.0 (HEKA Electronics, Lambrecht/Pfalz, Germany).

The patch pipettes contained 135 mM CsF, 10 mM NaCl, 5 mM HEPES with the pH adjusted to 7.0 with 1 M CsOH. The external bathing solution contained 30 mM NaCl, 5 mM CsCl, 25 mM D-glucose, 1 mM $MgCl_2$, 1.8 mM $CaCl_2$, 5 mM HEPES, 20 mM tetraethylammonium chloride, 70 mM tetramethylammonium chloride with the pH adjusted to 7.40 with 1 M tetraethylammonium hydroxide. Peptide toxin was dissolved in external solution, and about a 10-μl volume was applied by pressure injection with a microinjector (IM-5B, Narishige). All chemical reagents were purchased from Sigma.

Conformational Analysis of Synthetic Peptides—The synthetic peptide samples used for ^{1}H NMR spectrum analyses were dissolved in 500 μl of 20 mM deuterium sodium acetate buffer at pH 4.0. One-dimensional ^{1}H NMR spectra were obtained on S12A and R26A mutants at 295 K. One- and two-dimensional ^{1}H NMR spectra were acquired on K27A and R29A mutants at 295 K.

RESULTS

Structure Calculations and Evaluation of Native HNTX-IV—Sequence-specific resonance assignments were performed according to the standard procedures established by Wüthrich (13). All of the backbone protons and more than 95% of the side chain protons were identified. 583 intramolecular distance constraints and 14 dihedral constraints were used to calculate the structure of HNTX-IV by distance geometry and simulated annealing calculation with the program X-PLOR. A family of 20 accepted structures with lower energies and better Ramachandran plots were selected to represent the three-dimensional solution structure of HNTX-IV. A summary of the structural statistics for HNTX-IV is given in Table I. The structures have no distance violations greater than 0.2 Å and no dihedral violations greater than 2.0°. Furthermore they have favorable non-bonded contacts as evidenced by the low values of the mean Lennard-Jones potentials and good covalent geometry as indicated by the small deviations from ideal bond lengths and bond angles. Analysis of the structures in PROCHECK (17) shows that 85.3% of non-Pro, non-Gly residues lie in the most favored regions of the Ramachandran plot with a further 14.7% in additionally allowed regions.

Structure Description of Native HNTX-IV—Fig. 2*A* shows the best fit superposition of the backbone atoms (N, C_α, and C) for the 20 converged structures of native HNTX-IV. Analysis of the 20 converged structures indicated that the molecular structure of HNTX-IV contained a short triple-stranded antiparallel β-sheet formed by the strands Lys^7–Cys^9, Leu^{22}–Ser^{25} and Trp^{30}–Tyr^{33}, respectively (Fig. 2*B*). The information from strong sequential $d_{\alpha N}$ and weak d_{NN}, interstrand NOE connectivities, chemical shift index (18), large $^3J_{NH\text{-}C\alpha H}$ coupling constants, and slowly exchanging amide protons also occurred in a β-sheet. The turns in HNTX-IV were also identified using a standard definition that states that the distance between $C_\alpha(i)$ and $C_\alpha(i + 3)$ should be less than 7 Å and that the characteristic NOE connectivities of backbone protons (13) for the corresponding turn segments are presented. These analyses led to the identification of four β-turns (Fig. 2*B*), which were classified according to Richardson (19). The four β-turns involve residues Gly^4–Lys^7 (Type II), Pro^{11}–Asp^{14} (Type I), Lys^{18}–Asn^{21} (Type I), and Arg^{26}–Arg^{29} (Type I).

HNTX-IV adopts an inhibitor cystine knot motif commonly observed in toxic and inhibitory peptides (20). The cystine knot in HNTX-IV is formed by three disulfide bonds linked as Cys^2-Cys^{17}, Cys^9-Cys^{24}, and Cys^{16}-Cys^{31} in which the Cys^{16}-Cys^{31} disulfide bond passes through a 16-residue ring formed by the intervening polypeptide backbone and the Cys^2-Cys^{17} and Cys^9-Cys^{24} disulfide bonds.

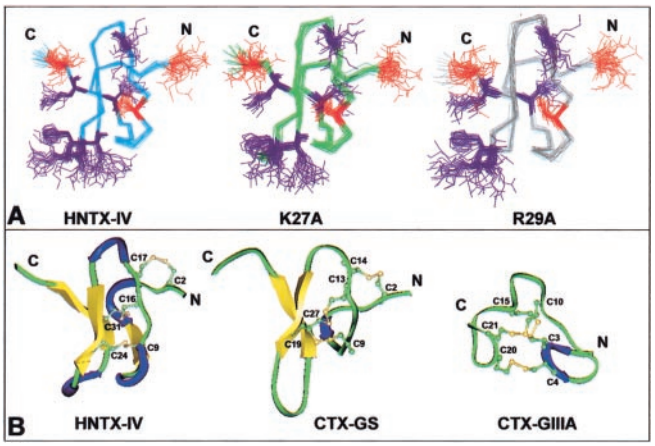

FIG. 2. **Structural comparison of HNTX-IV and correlated toxin molecules.** *A*, ensembles of 20 energy-refined conformers representing the solution structures of native HNTX-IV, K27A, and R29A. The backbones are shown in *cyan*, *green*, and *gray*, respectively. Positively charged side chains are shown in *blue*, and negatively charged side chains are shown in *red*. *B*, comparison of HNTX-IV to conotoxin GS (*CTX-GS*) and μ-conotoxin GIIIA (*CTX-GIIIA*) (conotoxin GS, Protein Data Bank code 1AG7; μ-conotoxin GIIIA, Protein Data Bank code 1TCG). The β-sheet is shown in *yellow*, the turn is shown in *blue*, and the random coil structure is shown in *green*. Three disulfide bonds of each molecule are indicated. The letters *N* and *C* refer to the amino and carboxyl termini, respectively.

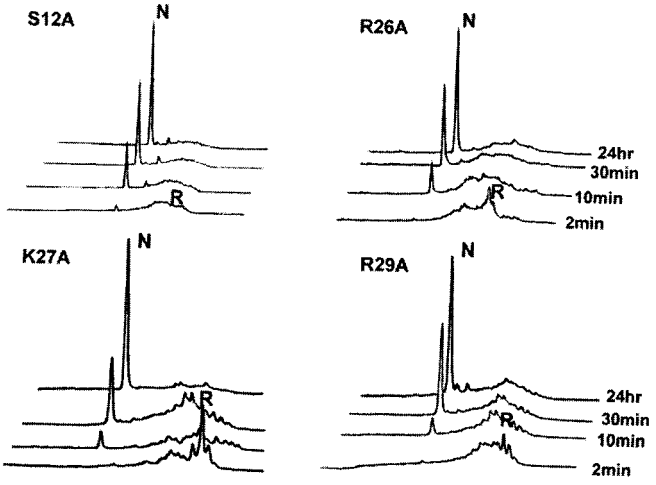

FIG. 3. **Analytical reverse-phase HPLC profiles of the oxidation products of S12A, R26A, K27A, and R29A at different times.** Oxidation was performed in 5 mM GSH, 0.5 mM GSSG, 0.1 M NaCl, 0.1 M Tris·HCl buffer, pH 7.4. *N* and *R* indicate isomers with three native and fully reduced disulfides, respectively.

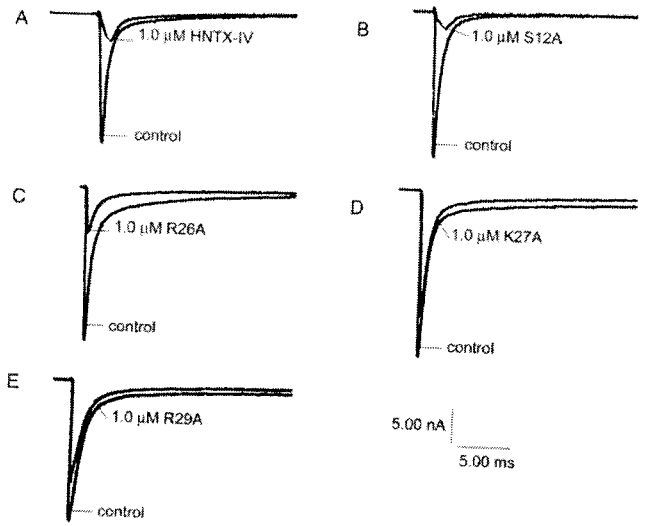

FIG. 4. **Effects of native HNTX-IV and four analogues at a concentration of 1.0 μM on TTX-S sodium channels in rat DRG neurons.** Current traces were evoked by depolarizations ranging from a holding potential of −80 to −20 mV. *A*, native HNTX-IV; *B*, S12A; *C*, R26A; *D*, K27A; *E*, R29A.

Peptide Synthesis and Characterization—Solid-phase synthesis of mutants S12A, R26A, K27A, and R29A, using Fmoc-protected amino acids and HOBt/TBTU coupling, yielded a major product as revealed by reverse-phase HPLC analysis and MALDI-TOF mass spectrometry. The purified reduced peptides were folded/oxidized in buffer 0.1 M Tris·HCl, 0.1 M NaCl, pH 7.4, containing 5 mM GSH, 0.5 mM GSSG for 24 h at room temperature. Purified products were homogeneous in analytical reverse-phase HPLC (Fig. 3), and their masses (3972.95 Da, 3903.45 Da, 3931.02 Da, and 3903.60 Da for S12A, R26A, K27A, and R29A, respectively) were in good accordance with the theoretical masses for all oxidized analogues.

Effects of Synthetic Analogues on Sodium Channel Currents—The biological activities of four analogues of HNTX-IV were studied by testing their capacity to inhibit the TTX-S sodium channels in rat DRG neurons. At a concentration of 1.0 μM, all analogues were observed to produce different inhibitions of the TTX-S sodium currents (Fig. 4). The dose-response curves shown in Fig. 5 illustrate the block of sodium channels at peptide concentrations ranging from 0.1 nM to 1.0 mM. The IC_{50} values of 58.3 and 99.6 nM were estimated for S12A and R26A, respectively. These values were approximately similar to that of native HNTX-IV (34.0 nM). In contrast, K27A and R29A caused reductions in potency of 2 orders of magnitude with estimated IC_{50} values of 3.22 and 6.93 μM, respectively. These results indicated that residues Ser^{12} and Arg^{26} of HNTX-IV were unimportant for activity, while Lys^{27} and Arg^{29} were necessary for its binding to TTX-S sodium channels.

Conformational Analysis of Synthetic Analogues—One- and two-dimensional ^1H NMR spectroscopy were used to analyze rigorously the structures of the synthetic analogues to determine the extent of isomer purity and to assess conformational integrity. The fact that one-dimensional ^1H NMR spectra of S12A and R26A (data not shown) were similar to that of native HNTX-IV suggests that the native folding was maintained for S12A and R26A mutants. However, the one-dimensional ^1H NMR spectra of K27A and R29A (data not shown), especially R29A, exhibited more differences from that of native HNTX-IV, so sequential assignments were performed from two-dimensional spectra for K27A and R29A mutants. As $C^{\alpha}H$ and NH chemical shifts are known to correlate with backbone conformation in proteins or peptides (21, 22), deviations in $C^{\alpha}H$ and NH chemical shifts from native HNTX-IV provide a useful reference of structural change upon mutation. NH chemical shift deviations from the native state are shown in Fig. 6. Although some deviations of the $C^{\alpha}H$ resonances also occurred in K27A and R29A, mainly R29A, the changes were found to be small, typically less than 0.1 ppm, with only two greater than 0.13 ppm. The deviations of $C^{\alpha}H$ chemical shifts were typically less than half the size of the NH deviations, and so no large changes in backbone conformation were expected for K27A and R29A, a fact in accord with the calculated structures of K27A and R29A.

A quantitative characterization of the structure determinations is given in Table I. The solution structures of K27A and R29A, as shown in Fig. 2*A*, belong to the inhibitor cystine knot structural family. The atomic root mean square (r.m.s.) difference of K27A and R29A from the native HNTX-IV was 0.742 and 0.732 Å, respectively, for the backbone atoms (N, C_{α}, and

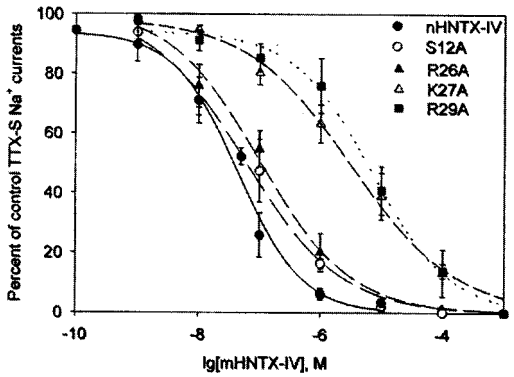

FIG. 5. **Dose-dependent curves illustrating the block of TTX-S sodium currents on rat DRG neurons by native HNTX-IV, S12A, R26A, K27A, and R29A.** Every data point (mean ± S.E.), which came from five to eight cells, shows current relative to control. Apparent IC_{50} values are as follows: native HNTX-IV, IC_{50} = 34.0 nM; S12A, IC_{50} = 58.3 nM; R26A, IC_{50} = 99.6 nM; K27A, IC_{50} = 3.22 μM; R29A, IC_{50} = 6.93 μM.

C) of all residues (Fig. 7*B*). The r.m.s. difference of two mutants was 0.440 Å for the backbone atoms (N, C_α, and C). The convergence of structures for the two synthetic analogues and native HNTX-IV did not differ significantly, suggesting that either the chemical properties or the conformations of their constituent amino acid side chains account for their different activities.

DISCUSSION

HNTX-IV and previously characterized HNTX-III, HNTX-V, and HWTX-IV have been shown to specifically inhibit the mammal neuronal TTX-S sodium channels. They seem to interact with neurotoxin receptor site 1 through a mechanism quite similar to that of TTX without affecting the activation and inactivation kinetics (7–9). Although we have not conducted an isotope-labeled toxin binding assay to test whether they share the same binding site with TTX or saxitoxin (23), we have demonstrated that among all reported spider toxins, the four toxins (HNTX-III–V and HWTX-IV) are a new class of depressant spider toxins affecting VGSCs. They could prove to be a class of novel, useful ligands to investigate the multiple molecular forms of VGSCs in vertebrates.

Previous studies on sodium channel blockers have revealed that 1) three-dimensional structures were essential for the activity, 2) one important characteristic required for blockage of sodium current was the presence of a positively charged region on the toxin, and 3) the guanidine group and hydroxyl group were important for the high inhibitory activity (24–27). The most well known example is μ-conotoxin GIIIA among neurotoxins acting at site 1 affecting VGSCs (24–30). Studies of site-directed mutagenesis in VGSCs and μ-conotoxin GIIIA/B have also been carried out to identify that the main acidic residues Glu^{758}, Asp^{762}, Glu^{765}, and Asp^{1241} at site 1 of VGSCs and residues Arg^{13}, Gln^{14}, Lys^{16}, Hyp^{17}, and Arg^{19} of μ-conotoxin GIIIA are involved in the binding and blocking activity (31, 32). Hence it seems clear that inhibitors bind to the sodium channels at least in part by electrostatic interactions or hydrogen bonds. HNTX-IV contains seven positively charged residues (Lys^7, Lys^{18}, Arg^{26}, Lys^{27}, His^{28}, Arg^{29}, and Lys^{32}) and three negatively charged residues (Glu^1, Asp^{14}, and Glu^{34}), producing a net positive charge (theoretical pI = 8.66) on this molecule (Fig. 2*A*). Evidently the positively charged side chains are located on the surface of the peptide. In particular, the surface of loop IV (Arg^{26}, Lys^{27}, His^{28}, and Arg^{29}) bears the majority of the positively charged residues with Arg^{26}, Lys^{27}, His^{28}, and Arg^{29} being the most solvent-exposed. In addition, similar to the essential hydroxyl groups of TTX (9-OH and 10-OH in TTX and geminal 12-OH groups in saxitoxin) and 4-trans-L-hydroxyproline in μ-conotoxins, the hydroxyl group of Ser^{12} is close to the important guanidine groups of Arg^{26} and Arg^{29} in HNTX-IV, and Ser^{12} is also quite solvent-exposed like these basic residues. The fact that the most solvent-exposed residues Arg^{26}, Lys^{27}, and Arg^{29} of loop IV and vicinal Ser^{12} in spatial position are extremely well conversed among the depressant toxins suggested the possibility that the residues Ser^{12}, Arg^{26}, Lys^{27}, and Arg^{29} in HNTX-IV were the crucial residues for its blocking activity. Fig 7*A*, *a* shows the surface profile of native HNTX-IV and the presentation identifying the four interesting residues. Based on the above analysis, we synthesized four analogues, S12A, R26A, K27A, and R29A, by solid-phase Fmoc chemistry.

Structure-Function Relationships of HNTX-IV—Generally the loss of activities of toxin mutants is mainly due to 1) the conformational change of toxins upon mutation or 2) the direct interaction of the mutated residues with the sodium channel molecules. The functional assays investigated in our study indicated that the S12A and R26A mutants were found to have activities near that of native HNTX-IV, while K27A and R29A demonstrated activities reduced by 2 orders of magnitude. One-dimensional ^1H NMR spectra suggested that S12A and R26A formed molecular conformations similar to that of native HNTX-IV. However, the one-dimensional ^1H NMR spectra of K27A and R29A, especially R29A, exhibited more differences from that of native HNTX-IV. To make it clear whether the residues Lys^{27} and Arg^{29} of HNTX-IV interact directly with Na^+ channel molecules or the residues are important for maintaining the correct local structures of the toxin, we elucidated the solution structures of the inactive mutants K27A and R29A. In fact, the structures obtained for K27A and R29A were very similar to that of native HNTX-IV for which atomic r.m.s. difference values were considerably smaller for the backbone atoms of all residues. Moreover, in the determined structures of K27A and R29A, the side chains of residues 27 and 29 were located in a spatial position identical to those of native HNTX-IV (Fig. 7*B*). Taken with the structure-activity data for the point mutants described here, conclusions were made that residues Ser^{12}, Arg^{26}, Lys^{27}, and Arg^{29} were not responsible for stabilizing the distinct conformation of HNTX-IV and Ser^{12} and Arg^{26} appeared unimportant for HNTX-IV binding to the TTX-S VGSCs, but Lys^{27} and Arg^{29} were critical for the bioactivities. The detailed NMR investigation of the inactive analogue structures showed that the decrease in the blocking activity was primarily the result of the loss of positively charged side chain interactions with the binding site of sodium channels rather than the conformational change associated with the substitutions.

Previously it was mentioned that the mainly acidic residues in Na^+ channel molecules interacted with basic residues and vicinal polar amino acids in toxins via electrostatic interactions or hydrogen bonds. Residues Lys^{27} and Arg^{29} in HNTX-IV are positively charged residues with long side chains, hence it is plausible that the positive charges of two residues are an important factor for its binding to TTX-S VGSCs, similar to the function of basic residues in μ-conotoxin GIIIA. As a result, the electrostatic potentials seem to play an important role in conducting the block of the TTX-S Na^+ channels by HNTX-IV.

Many studies have revealed that the binding interface of the toxin molecule is rather wide, and multiple amino acid residues of toxins are involved in the interaction with Na^+ channels (5, 6, 25). The NMR structure of HNTX-IV displayed that Ser^{12}, Arg^{26}, Lys^{27}, and Arg^{29} were clustered on one side of the molecule with their side chains being more surface-exposed

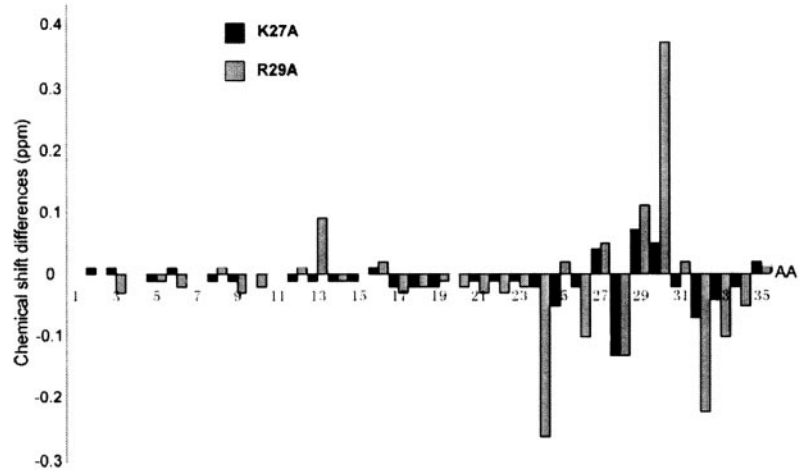

FIG. 6. **Chemical shift differences of K27A and R29A from native HNTX-IV, respectively.**

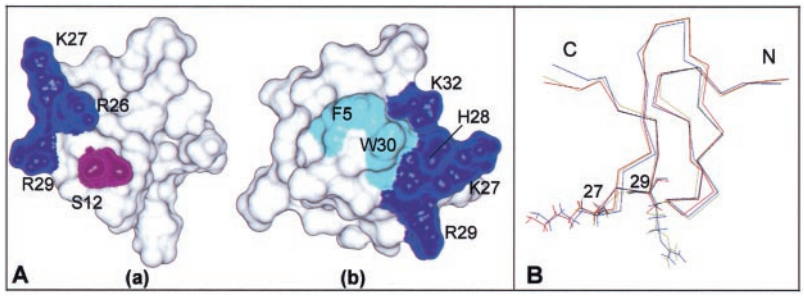

FIG. 7. **Solution structure characterization of HNTX-IV.** *A*, surface profile of HNTX-IV. *a*, surface profile of predicted active sites. *b*, surface profile of putative active sites. *Blue*, *mauve*, and *cyan* regions represent positively charged, polar, and hydrophobic residues, respectively. *B*, backbone superposition of native HNTX-IV (*blue*), K27A (*green*), and R29A (*red*). *27* and *29* indicate the positions of substituted amino acid residues. The fit was done using the common secondary structure elements. The letters *N* and *C* refer to the amino and carboxyl termini, respectively.

(Fig. 7*A*, *a*). Unexpectedly our present results showed that mutations of only Lys^{27} and Arg^{29} to Ala had large effects on HNTX-IV binding to TTX-S Na^+ channels. Therefore, we hypothesize that HNTX-IV binds to the sodium channels with the surface encompassing mainly Lys^{27} and Arg^{29}, as well as other uncharacterized residues, but not the surface formed by Ser^{12}, Arg^{26}, Lys^{27}, and Arg^{29}. After comparison of these structures and activities with the correlated toxins, we proposed that residues Lys^{27} and Arg^{29} and vicinal residues His^{28}, Lys^{32}, Phe^5, and Trp^{30} localized on one face of HNTX-IV (Fig. 7*A*, *b*) were responsible for binding to TTX-S VGSCs in rat DRG neurons.

Structural Comparison of HNTX-IV with μ-Conotoxins—μ-Conotoxins are receptor site 1 sodium channel blockers purified from the venom of marine cone snails that act selectively to occlude the pore of VGSCs by competing with TTX and saxitoxin. Among the μ-conotoxins, GIIIA/B and GS specifically inhibit rat skeletal muscle sodium channels (rNa(v)1.4), whereas PIIIA inhibits neuronal as well as muscle TTX-S sodium channels (33–39). The three-dimensional structure of HNTX-IV has little resemblance to the three-loop μ-conotoxins (GIIIA/B and PIIIA) in agreement with the low sequence identity between them and their different cystine frameworks (27, 40, 41). Unlike the three-loop μ-conotoxins, both conotoxin GS and HNTX-IV belong to the inhibitor cystine knot structural family with the same disulfide bond pattern despite little sequence identity (42). Fig. 2*B* shows the secondary structures of HNTX-IV, conotoxin GS, and μ-conotoxin GIIIA. The main structure of the three-loop μ-conotoxins is composed of a small β-hairpin, a distorted 3_{10} helix comprising residues 13–22, and several turns, whereas HNTX-IV and conotoxin GS consist mainly of β-strands and turns. Further structural comparison of HNTX-IV with conotoxin GS reveals that although the two molecules contain a Type II β-turn in loop I, several local differences in backbone conformation are observed. First, in HNTX-IV, the first strand constitutes a complete β-sheet at Lys^7–Cys^9, whereas in conotoxin GS it consists solely of a β-bridge at Ser^7. Second, the size of loops II and IV is strikingly different between the two molecules. In particular, loop II of conotoxin GS lacks three residues relative to HNTX-IV and has a markedly different conformation. Moreover another distinct difference is observed in the relative orientation of loops II and IV in these two structures. Such differences in local structures and in the amino acid sequences between HNTX-IV and μ-conotoxins may play a vital role in discriminating the specific target subtype of sodium channels.

Conclusion—In conclusion, the solution structure of HNTX-IV determined by ^1H NMR proved that the molecule adapted a typical inhibitor cystine knot motif. Based on the predicted active sites, we synthesize four analogues of HNTX-IV followed by structural elucidation of two inactive mutants. The solution structure of native HNTX-IV and its inactive analogues reported here should provide a basis for the further understanding of the structure-activity relationships of these toxins like HNTX-IV and insight into the structural difference of different subtypes of VGSCs.

Acknowledgment—We are grateful to Guangzhong Tu of Beijing Institute of Microchemistry for collecting the ^1H NMR spectra.

REFERENCES

1. Hodgkin, A. L., and Huxley, A. F. (1952) *J. Physiol.* **117,** 500–544
2. Catterall, W. A. (2000) *Neuron* **26,** 13–25
3. Yu, F. H., and Catterall, W. A. (2003) *Genome Biol.* http://genomebiology.com/2003/4/3/207
4. Yu, F. H., Westenbroek, R. E., Silos-Santiago, I., McCormick, K. A., Lawson,

D., Ge, P., Ferriera, H., Lilly, J., DiStefano, P. S., Catterall, W. A., Scheuer, T., and Curtis, R. (2003) *J. Neurosci.* **23,** 7577–7585
5. Cestèle, S., and Catterall, W. A. (2000) *Biochimie* (*Paris*) **82,** 883–892
6. Escoubas, P., Diochot, S., and Corzo, G. (2000) *Biochimie* (*Paris*) **82,** 893–907
7. Liu, Z. H., Dai, J., Chen, Z. R., Hu, W. J., Xiao, X. C., and Liang, S. P. (2003) *Cell. Mol. Life Sci.* **60,** 972–978
8. Peng, K., Shu, Q., Liu, Z. H., and Liang, S. P. (2002) *J. Biol. Chem.* **277,** 47564–47571
9. Xiao, Y. C., and Liang, S. P. (2003) *Toxicon* **41,** 643–650
10. Fuhrman, F. A. (1967) *Sci. Am.* **217,** 60–71
11. Liu, Z. H., Chen, P., and Liang, S. P. (2002) *Acta Biochim. Biophys. Sin.* **34,** 516–519
12. Li, D. L., Xiao, Y. C., Hu, W. J., Xie., J. Y., Bosmans, F., Tytgat, J., and Liang, S. P. (2003) *FEBS Lett.* **555,** 616–622
13. Wüthrich, K. (1986) *NMR of Protein and Nucleic Acids*, John Wiley & Sons, Inc., New York
14. Brünger, A. T. (1992) *X-PLOR Manual*, Version 3.1, Yale University, New Haven, CT
15. Zhu, Q., Liang, S. P., Martin, L., Gasparini, S., Ménez, A., and Vita, C. (2002) *Biochemistry* **41,** 11488–11494
16. Hu, H. Z., and Li, Z. W. (1997) *J. Physiol.* **501,** 67–75
17. Laskowski, R. A., Rullmannn, J. A., MacArthur, M. W., Kaptein, R., and Thornton, J. M. (1996) *J. Biomol. NMR* **8,** 477–486
18. Wishart, D. S., Sykes, B. D., and Richards, F. M. (1992) *Biochemistry* **31,** 1647–1651
19. Richardson, J. S. (1981) *Adv. Protein Chem.* **34,** 167–236
20. Pallaghy, P. K., Nielsen, K. J., Craik, D. J., and Norton, R. S. (1994) *Protein Sci.* **3,** 1833–1839
21. Szilágyi, L., and Jardetzky, O. (1989) *J. Magn. Reson.* **83,** 441–449
22. Wishart, D. S., Sykes, B. D., and Richards, F. M. (1991) *J. Mol. Biol.* **222,** 311–333
23. Schantz, E. J. (1986) *Ann. N. Y. Acad. Sci.* **479,** 15–23
24. Sato, K., Ishida, Y., Wakamatsu, K., Kato, R., Honda, H., Ohizumi, Y., Nakamura, H., Ohya, M., Lancelin, J. M., and Kohda, D. (1991) *J. Biol. Chem.* **266,** 16989–16991
25. Wakamatsu, K., Kohda, D., Hatanaka, H., Lancelin, J. M., Ishida, Y., Oya, M., Nakamura, H., Inagaki, F., and Sato, K. (1992) *Biochemistry* **31,** 12577–12584
26. Becker, S., Prusak-Sochaczewski, E. P., Zamponi, G., Beck-Sickinger, A. G., Gordon, R. D., and French, R. J. (1992) *Biochemistry* **31,** 8229–8238
27. Lancelin, J. M., Kohda, D., Tate, S., Yanagawa, Y., Abe, T., Satake, M., and Inagaki, F. (1991) *Biochemistry* **30,** 6908–6916
28. Nakamura, M., Niwa, Y., Ishida, Y., Kohno, T., Sato, K., Oba, Y., and Nakamua, H. (2001) *FEBS Lett.* **503,** 107–110
29. Li, R. A., Sato, K., Kodama, K., Kohno, T., Xue, T., Tomaselli, G. F., and Marbán, E. (2002) *FEBS Lett.* **511,** 159–164
30. Hui, K., Lipkind, G., Fozzard, H. A., and French, R. J. (2002) *J. Gen. Physiol.* **119,** 45–54
31. Li, R. A., Ennis, I. L., Vélez, P., Tomaselli, G. F., and Marbán, E. (2000) *J. Biol. Chem.* **275,** 27551–27558
32. Li, R. A., Ennis, I. L., French, R. J., Dudley, S. C., Jr., Tomaselli, G. F., and Marbán, E. (2001) *J. Biol. Chem.* **276,** 11072–11077
33. Cruz, L. J., Gray, W. R., Olivera, B. M., Zeikus, R. D., Kerr, L., Yoshikami, D., and Moczydlowski, E. (1985) *J. Biol. Chem.* **260,** 9280–9288
34. Yanagawa, Y., Abe, T., and Satake, M. (1987) *J. Neurosci.* **7,** 1498–1502
35. Yanagawa, Y., Abe, T., Satake, M., Odani, S., Suzuki, J., and Ishikawa, K. (1988) *Biochemistry* **27,** 6256–6262
36. Moczydlowski, E., Olivera, B. M., Gray, W. R., and Strichartz, G. R. (1986) *Proc. Natl. Acad. Sci. U. S. A.* **83,** 5321–5325
37. Li, R. A., Tsushima, R. G., and Backx, P. H. (1997) *Biophys. J.* **73,** 1874–1884
38. Shon, K. J., Olivera, B. M., Watkins, M., Jacobsen, R. B., Gray, W. R., Floresca, C. Z., Cruz, L. J., Hillyard, D. R., Brink, A., Terlau, H., and Yoshikami, D. (1998) *J. Neurosci.* **18,** 4473–4481
39. Safo, P., Rosenbaum, T., Shcherbatko, A., Choi, D.Y., Han, E., Toledo-Aral, J. J., Olivera, B. M., Brehm, P., and Mandel, G. (2000) *J. Neurosci.* **20,** 76–80
40. Hill, J. M., Alewood, P. F., and Craik, D. J. (1996) *Biochemistry* **35,** 8824–8835
41. Nielsen, K. J., Watson, M., Adams, D. J., Hammarstrom, A. K., Gage, P. W., Hill, J. M., Craik, D. J., Thomas, L., Adams, D., Alewood, P. F., and Lewis, R. J. (2002) *J. Biol. Chem.* **277,** 27247–27255
42. Hill, J. M., Alewood, P. F., and Craik, D. J. (1997) *Structure* **15,** 571–583